Journal of Organometallic Chemistry 695 (2010) 1541–1549

Contents lists available at ScienceDirect

Journal of Organometallic Chemistry

journal homepage: www.elsevier.com/locate/jorganchem

Ferrocenyl phosphane nickel carbonyls: Synthesis, solid state structure, and their use as catalysts in the oligomerization of ethylene

Dieter Schaarschmidt [a], Janett Kühnert [a], Sascha Tripke [a], Helmut G. Alt [b], Christian Görl [b], Tobias Rüffer [a], Petra Ecorchard [a], Bernhard Walfort [a], Heinrich Lang [a,*]

[a] Technische Universität Chemnitz, Fakultät für Naturwissenschaften, Institut für Chemie, Lehrstuhl für Anorganische Chemie, Straße der Nationen 62, 09111 Chemnitz, Germany
[b] Laboratorium für Anorganische Chemie, Universität Bayreuth, Postfach 10 12 51, 95440 Bayreuth, Germany

ARTICLE INFO

Article history:
Received 15 December 2009
Received in revised form 3 March 2010
Accepted 7 March 2010
Available online 21 March 2010

Dedicated to Professor Hubert Schmidbaur on the occasion of his 75th birthday

Keywords:
Nickel carbonyls
Ferrocenyl phosphanes
Oligomerization of ethylene
Homogeneous catalysis
Heterogeneous catalysis

ABSTRACT

The synthesis of diverse ferrocenyl phosphane nickel carbonyls of type $(FcPPh_2)Ni(CO)_3$ (**3**), $(FcPPh_2)_2Ni(CO)_2$ (**4**), $fc(PR_2Ni(CO)_3)_2$ (R = Ph (**6a**), R = *p*-tolyl (**6b**)), and $(fc(PPh_2)_2)Ni(CO)_2$ (**7**) (Fc = (η^5-C_5H_5)(η^5-C_5H_4)Fe, fc = (η^5-C_5H_4)$_2$Fe) starting from $FcPPh_2$ (**1**), $fc(PR_2)_2$ (R = Ph (**5a**); R = *p*-tolyl (**5b**)), and $Ni(CO)_4$ (**2**) is described. The structures of **3**, **4**, **6b**, and **7** in the solid state are reported, intermolecular interactions by π–π-contacts are discussed. The behavior of **3**, **4**, **6a**, **6b**, and **7** towards the oligomerization of ethylene is reported. All compounds, except **4**, were found to be inactive in homogeneous ethylene oligomerization, while they exhibit moderate activities (up to 660 kg prod/mol Ni h) in heterogeneous ethylene oligomerization experiments.

1. Introduction

Nickel phosphanes have attracted considerable interest in recent years because they can be applied successfully in homogeneous catalysis including the polymerization of formaldehyde [1,2], dimerization of propene [3–11], synthesis of α-olefines [12–19], asymmetric hydrocyanation of styrene [20,21], hydrogenolysis of biphenylene [22,23], and the coupling of Grignard reagents with chloropyrimidines [24,25] and aryl chlorides [26,27]. Due to their diverse applications in the field of material sciences, e.g. the synthesis of semi-conductive nickel phosphane coordination polymers [28] and the generation of nickel nanoparticles from nickel carbonyls [29–33], nickel-containing compounds are of topical interest.

Focusing on one topic, the oligomerization of α-olefins is possible by using catalytically active nickel systems, i.e. [((η^5-$C_5H_4C(H)$=NPh)(η^5-$C_5H_4P^tBu_2$)Fe)NiCl] [34], [(1,5-cod)$_2$Ni] (cod = cyclooctadiene) [35], and [((η^5-$C_5H_4C(H)$=N(C_6F_5))(η^5-$C_5H_4PPh_2$)Fe)$_2$Ni(CO)$_2$] [36]. In 1976, Yoo [37] described the heterogeneous oligomerization of α-olefins catalyzed by triphenylphosphane nickel carbonyls, while Wu [38] demonstrated the oligomerization potential of the same complexes in homogeneous reactions. Lately, Weng et al. have reported that nickel(0) compounds show high catalytic activity and selectivity towards α-olefins in ethylene oligomerization, although they are more sensitive compared to nickel(II) compounds [34,36,39,40].

This prompted us to prepare a series of different di- and trimetallic ferrocenyl phosphane-based nickel carbonyls and to screen their catalytic activities in α-olefin oligomerization reactions.

2. Results and discussion

Complexes $(FcPPh_2)Ni(CO)_3$ (**3**) (Fc = (η^5-C_5H_5)(η^5-C_5H_4)Fe) and $fc(PR_2Ni(CO)_3)_2$ (fc = (η^5-C_5H_4)$_2$Fe; R = Ph (**6a**); R = *p*-tolyl (**6b**)) are accessible by treatment of the phosphino ferrocenes $FcPPh_2$ (**1**) and $fc(PR_2)_2$ (R = Ph (**5a**); R = *p*-tolyl (**5b**)) with an excess of $Ni(CO)_4$ (**2**) in petroleum ether at ambient temperature (Fig. 1). When the stoichiometry of **1** and **2** is changed to 2:1 $(FcPPh_2)_2Ni(CO)_2$ (**4**) could be isolated. The introduction of a third $FcPPh_2$ group was not possible which is attributed to electronic reasons as outlined elsewhere [41]. The more phosphane ligands are present, the stronger the Ni–C_{CO} bonds are. Organometallics **3** and **4** are orange solid materials which are stable under inert gas atmosphere. Under aerobic conditions they slowly decompose to give elemental nickel and the respective ferrocenyl phosphanes. In contrast, compounds **6a** and **6b** gradually decompose even under inert gas atmosphere within days. Heating **6a** in toluene

* Corresponding author. Tel.: +49 371 531 21210; fax: +49 371 531 21219.
E-mail address: heinrich.lang@chemie.tu-chemnitz.de (H. Lang).

0022-328X/$ - see front matter © 2010 Elsevier B.V. All rights reserved.
doi:10.1016/j.jorganchem.2010.03.012

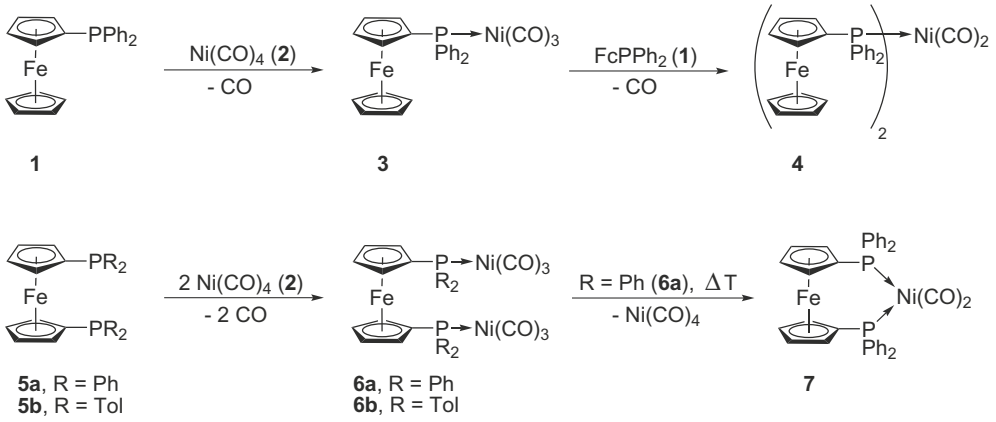

Fig. 1. Synthesis of **3**, **4**, **6a**, **6b**, and **7** from **1**, **5a**, **5b**, and **2**.

gave (fc(PPh$_2$)$_2$)Ni(CO)$_2$ (**7**) (Fig. 1), firstly synthesized by Vasapollo et al. [42] and Hamann and Hartwig [43].

Compounds **3**, **4**, **6**, and **7** were characterized by NMR (^{1}H and ^{31}P{^{1}H}) and IR spectroscopy proving the formation of ferrocenyl phosphane nickel carbonyls. Additionally, the structures of **3**, **4**, **6b**, and **7** in the solid state were determined by single crystal X-ray diffraction analysis.

The ^{1}H NMR spectral properties of **3**, **4**, **6**, and **7** are in accordance with their formulations as ferrocenyl phosphane-substituted nickel carbonyls showing the respective resonance patterns for the cyclopentadienyl and phenyl moieties. Most distinctive for **3** and **4** is the appearance of a broadened singlet for the C_5H_5 protons. All compounds exhibit broad signals for the $C_5H_4PR_2$ protons between 3.9 and 4.5 ppm, due to metallic nickel impurities on a sub-microgram scale.

Table 1
IR ν_{CO} (KBr) and ^{31}P{^{1}H} NMR ($CDCl_3$) data of **3**, **4**, **6a**, **6b**, and **7**.

Compd	ν_{CO} (cm^{-1})	^{31}P{^{1}H} (ppm)
3	1984, 2066	23.0
4	1927, 1989	28.7
6a	1985, 2067	22.6
6b	1980, 2066	19.7
7	1943, 2000	25.1

The ^{31}P{^{1}H} NMR spectra of **3**, **4**, **6**, and **7** show the expected resonances at 23.0 (**3**), 28.7 (**4**), 22.6 (**6a**), 19.7 (**6b**) and 25.1 ppm (**7**) owing to the coordination of the ferrocenyl phosphane moieties to a Ni(CO)$_x$ (x = 2, 3) fragment. Compared to the starting materials (−16.8 (**1**), −18.2 (**5a**), −20.1 (**5b**)) a shift to lower field is observed. The largest down-field shifts are found for compounds L_2Ni(CO)$_2$ (**4**, **7**), whereas **4** is less shielded.

Representative IR absorptions for the Ni(CO)$_x$ building blocks in **3**, **4**, **6**, and **7** are found between 1925 and 2070 cm^{-1} (Table 1), whereby the nickel carbonyl units display the characteristic CO absorption patterns according to their C_{2v} or C_{3v} symmetry [43–46]. The symmetric CO stretching frequency A_1 depends both on the nature and the number of the coordinated phosphane ligands [47,48]. From Table 1 it can be seen that the phosphanes exhibit almost identical donating properties (**3**, **6a** and **6b**), though significant differences are found, when mono- and di-substituted complexes are compared (**3** and **6a** vs. **4** and **7**). Strongest Ni–C bonds are observed for non-chelating donors as given in **4**, which is more likely attributed to steric than to eletronic reasons (vide infra).

The structures of **3** (Fig. 2), **4** (Fig. 3), **6b** (Fig. 4) and **7** (Fig. 5) in the solid state were determined by single crystal X-ray diffraction analysis. Single crystals could be obtained by cooling concentrated dichloromethane–toluene (**3**, **6b**, **7**) or petroleum ether–toluene mixtures (**4**) to −30 °C. Relevant crystallographic and structure

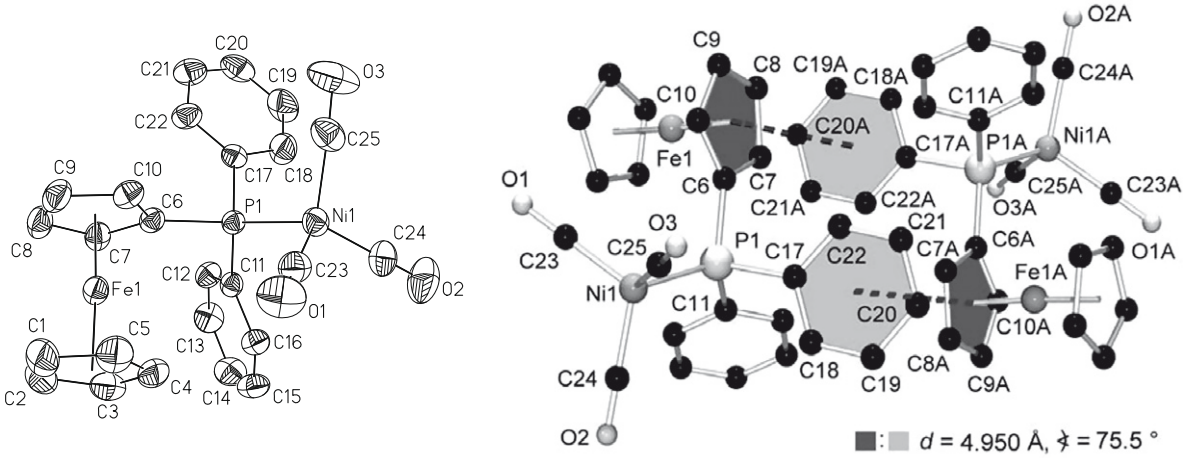

Fig. 2. Left: ORTEP diagram (50% probability level) of **3′** with the atom numbering scheme (hydrogen atoms are omitted for clarity). Right: Graphical representation of the π–π-interactions (dotted lines) between centrosymmetric pairs of **3′** (hydrogen atoms are omitted for clarity), where d refers to the center-to-center distance and ∢ refers to the inter-planar angle of the cyclopentadienyl C6–C10 and the phenyl ring C17A–C22A. Label 'A' refers to atoms of a first symmetry generated molecule of **3′**. Found π–π-interactions for related planes in **3″**: d = 5.016 Å, ∢ = 79.3°.

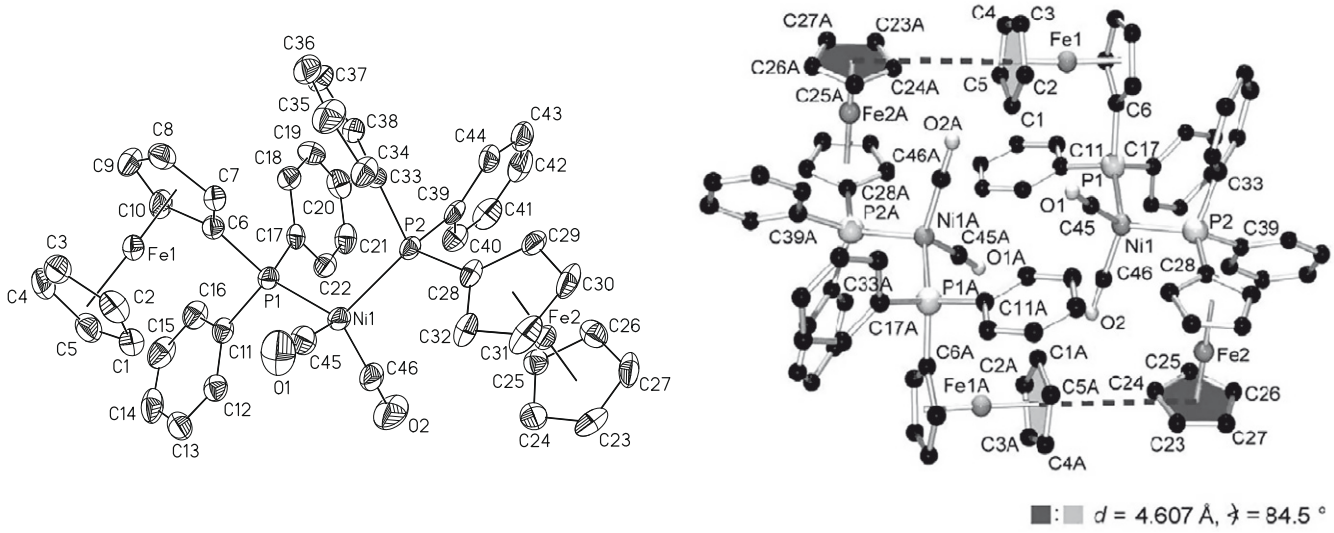

Fig. 3. Left: ORTEP diagram (50% probability level) of **4** with the atom numbering scheme (hydrogen atoms are omitted for clarity). Right: Graphical representation of the π–π-interactions (dotted lines) between centrosymmetric pairs of **4** (hydrogen atoms are omitted for clarity), where *d* refers to the center-to-center distance and $\measuredangle$ refers to the inter-planar angle of the cyclopentadienyl rings of the atoms C1–C5 and C23A–C27A. Label 'A' refers to atoms of a first symmetry generated molecule of **4**.

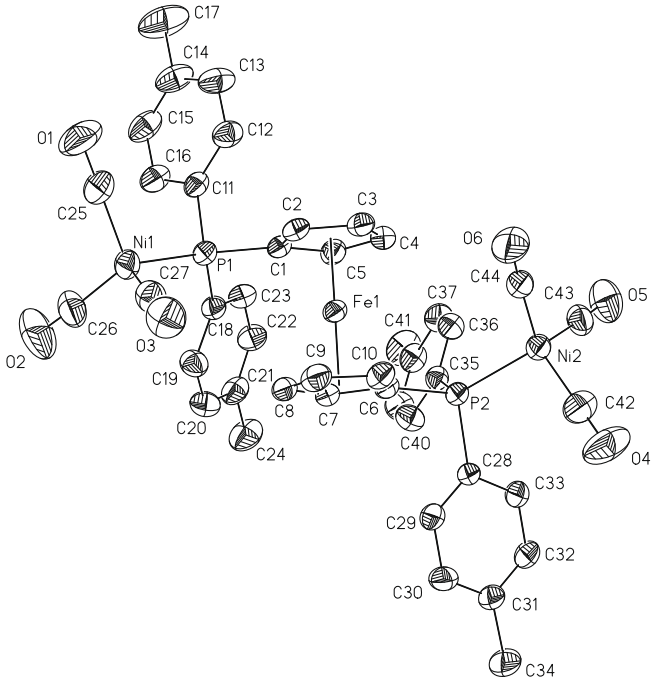

Fig. 4. ORTEP diagram (50% probability level) of **6b**′ with the atom numbering scheme (hydrogen atoms are omitted for clarity).

refinement data are summarized in Table 5. Representative bond distances (Å) and angles (°) are given in Table 2.

The asymmetric unit cell of **3** contains two (molecules **3**′ and **3**″) and that of **6b** one and a half crystallographic independent molecules (molecules **6b**′ and **6b**″). Molecule **6b**″ possesses a crystallographic imposed inversion symmetry with the inversion center on Fe2. Related bond distances of the two independent molecules **3**′ and **3**″ as well as **6b**′ and **6b**″ are identical within their mean deviations, while apparently differences for the related bond angles up to 3.5% are found for the independent molecules of **3** and **6** (Tables 2 and S1 (Supplementary material)). Therefore, only the bond lengths of molecules **3**′ and **6b**′ are discussed, whereas essential bond angles are disputed for each molecule.

Organometallics **3**, **4**, **6b**, and **7** show the expected tetrahedral ligand coordination around the nickel atom (Figs. 2–5). The cyclopentadienyl rings of all ferrocenes exhibit an almost coplanar conformation showing dihedral angles of their calculated mean planes of 2.8(2) (**3**′), 3.2(2) (**3**″), 1.8(3) and 0.3(3) (**4**), 0.9(2) (**6b**′), 0.0 (**6b**″) and 2.0(4)° (**7**) not influenced by mono-dentate (**3**, **4**, **6b**) or chelating (**7**) coordinations. The cyclopentadienyl rings are rotated by 12.3 (**3**′), 12.1 (**3**″), 17.5 (**4** with Fe1), and 14.8° (**6b**′), while the rotation angle of the second ferrocenyl unit in **4** (1.4° (with Fe2)) reveals an almost eclipsed conformation. Unlike, in **7** and **6b**″ rotation angles of 35° and 36° are found, illustrating a staggered conformation of the ferrocenes.

Compounds **3**, **4**, and **7** form centrosymmetric dimers of adjacent molecules in the solid state by π–π-interactions between one cyclopentadienyl and one phenyl (**3**), two cyclopentadienyl (**4**), or two phenyl rings (**7**). Geometrical details given in Figs. 2, 3 and 5 are closely related to T-shaped benzene dimers (*d* = 4.96 Å) [49]. Probably these π-contacts cause the different twisting of the two ferrocenyl moieties in **4**.

The observed Ni–C and Ni–P bond distances are in the range as reported for similar phosphane–Ni(CO)$_x$ compounds (x = 2, 3), i.e. [((η^6-C_6H_6)(η^6-$C_6H_5PMe_2$)Cr)$_2$Ni(CO)$_2$] (Ni–P, 2.207(2), 2.217(2); Ni–C, 1.747(6), 1.786(7) Å) [50], and [(2, 4, 6-C(CH$_3$)$_3$C$_6$H$_2$P-(η^2–Me$_3$SiC=CSiMe$_3$))Ni(CO)$_3$] (Ni–P, 2.276(1); Ni–C, 1.783(3), 1.798(3), 1.794(3) Å) [51]. Compared with **4** the Ni–P and Ni–C separations in **3**′ are slightly longer. This means that the more phosphane substituents and hence, less CO donors are present around the nickel atom, the shorter the Ni–C and Ni–P bonds. This is in full agreement with IR spectroscopy (vide supra).

The steric demand of a phosphane ligand can be expressed with the commonly used concept of the Tolman cone angle [47,52]. The Tolman cone angle allows to evaluate the catalytic activity of organometallics, as described elsewhere [52–54]. The cone angles were calculated to 167 (**3**′), 169 (**3**″), 180 (**4** with P1), 162 (**4** with P2), 166 (**6b**′ with P1), 170 (**6b**′ with P2), 166 (**6b**″), 163 (**7** with P1), and 153° (**7** with P2) (Table 3) using the program STERIC [55,56] implying larger cone angles than PPh$_3$ (145°) [47]. Obviously ferrocenyl moieties require more space than phenyl groups. Cone angles of **3**, **4** (with P2), and **6** agree well, while the cone angle of **4** (with P1) deviates more than 10°, which may be attributed to π-contacts (vide supra).

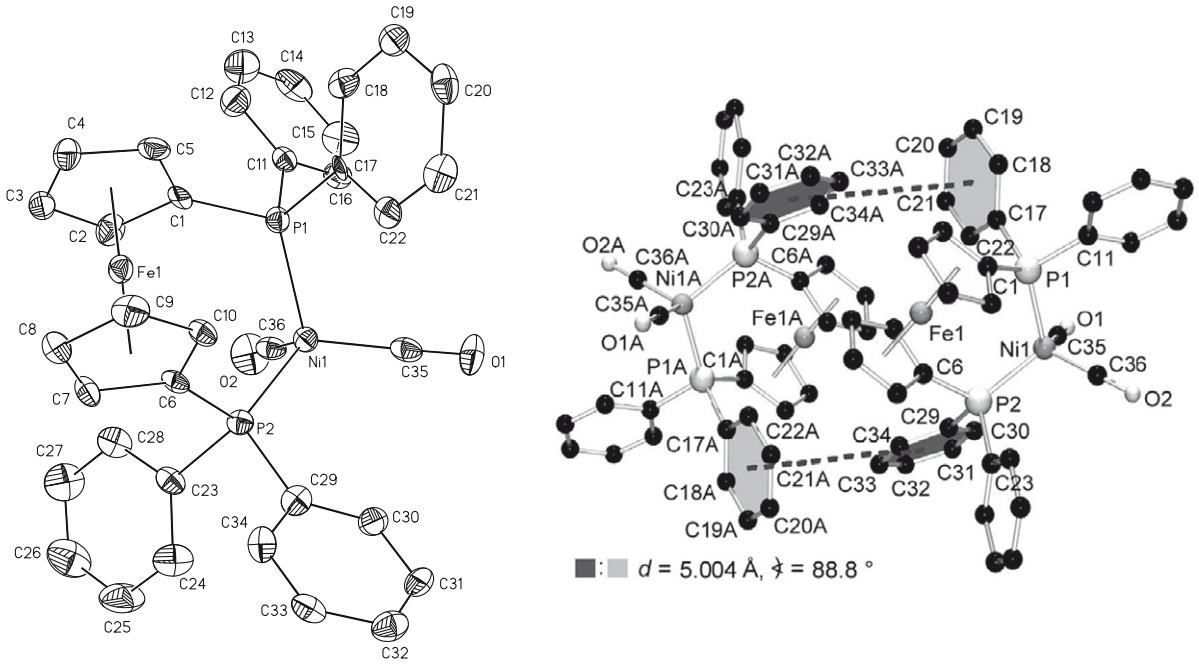

Fig. 5. Left: ORTEP diagram (50% probability level) of **7** with the atom numbering scheme (hydrogen atoms and the non-coordinating CH_2Cl_2 molecule are omitted for clarity). Right: Graphical representation of the π–π-interactions (dotted lines) between centrosymmetric pairs of **7** (hydrogen atoms are omitted for clarity), where *d* refers to the center-to-center distance and ∢ refers to the inter-planar angle of the phenyl rings of the atoms C17–C22 and C29A–C34A. Label 'A' refers to atoms of a first symmetry generated molecule of **7**.

Table 2
Selected bond distances (Å) and angles (°) for **3**, **4**, **6b**, and **7**.[a]

3′		**3″**		**4**		**6b′**		**6b″**		**7**	
Ni–P bond distances											
Ni1–P1	2.2260(6)	Ni2–P2	2.2263(6)	Ni1–P1	2.2161(12)	Ni1–P1	2.2234(12)	Ni3–P3	2.2266(11)	Ni1–P1	2.206(2)
				Ni1–P2	2.2204(12)	Ni2–P2	2.2280(11)			Ni1–P2	2.211(2)
Ni–C bond distances											
Ni1–C23	1.792(3)	Ni2–C48	1.785(3)	Ni1–C45	1.780(5)	Ni1–C25	1.779(6)	Ni3–C64	1.776(6)	Ni1–C35	1.756(7)
Ni1–C24	1.802(3)	Ni2–C49	1.796(3)	Ni1–C46	1.773(5)	Ni1–C26	1.773(6)	Ni3–C65	1.765(5)	Ni1–C36	1.771(7)
Ni1–C25	1.793(3)	Ni2–C50	1.797(3)			Ni1–C27	1.764(6)	Ni3–C66	1.778(6)		
						Ni1–C42	1.792(6)				
						Ni1–C43	1.755(6)				
						Ni1–C44	1.792(5)				
Bond angles											
				P1–Ni1–P2	110.98(4)					P1–Ni1–P2	108.19(8)

[a] Standard uncertainties are given in the last significant figure(s) in parenthesis.

Table 3
Summary of Tolman cone angles of **3**, **4**, **6b**, and **7**.

Compound	Tolman cone angle Θ (°)[a]
3	167 (**3′**), 169 (**3″**)
4	180 (with P1), 162 (with P2)
6b	161 (**6b′** with P1), 170 (**6b′** with P2), 166 (**6b″**)
7	163 (with P1), 153 (with P2)

[a] Tolman cone angles have been determined using STERIC.

For chelating ligands P–M–P bite angles are commonly used to discuss their steric characteristics [57]. There is some evidence that these angles affect the activity in catalytic reactions [58] including aminations [43], hydrocyanations [51], and ethylene oligo-/polymerizations [59]. For **7**, the P1–Ni1–P2 angle is 108.19(8)° (Table 2) which is similar to values observed for related molecules [60,61] and even non-chelating systems such as **4** (110.98(4)°).

Considering the relatively large cone angles of the phosphanes **1**, **5a**, and **5b** as well as the P–Ni–P bite angles of **4** and **7** near to ideal tetrahedral geometry it is obvious that the nickel carbonyls form catalysts rather for ethylene oligomerization than for polymerization [59].

Comparing the Tolman cone angles of **1** and **5a** with the P–Ni–P bite angles of **4** and **7**—the bite angle in **4** and **7** (Table 2) is almost identical whereas $FcPPh_2$ (**1**) seems to have a distinctively larger Tolman cone angle than $fc(PPh_2)_2$ (**5a**) (Table 3)—reveals that these two methods may give different results concerning steric parameters. The question arising from this observation is whether the Tolman model or the bite angle concept allows a more serious prediction of catalytic activity in ethylene oligomerization.

Compounds **3**, **4**, **6a**, and **7** were applied for both, homogeneous and heterogeneous ethylene oligo-/polymerization experiments. For blank tests, samples of the appropriate compounds were dissolved in a small amount of toluene (5 mL) and *n*-pentane (250 mL) and subjected to an ethylene pressure of 10 bar in a 1 L

Büchi steel reactor without the addition of a cocatalyst. The reaction temperature was set to 60 °C. As expected, no oligomerization products were obtained (entries 1–4, Table 4). Due to the excess of ethylene, the CO ligands at the nickel center may have been replaced by ethylene, however, there is no accessible metal–carbon bond into which the ethylene molecules can be inserted.

For the ethylene oligomerization experiments in homogeneous reactions the appropriate complexes were activated with methylaluminoxane (MAO) at a rate of Ni:Al = 1:2500. In contrast to the activation of metallocenes or other metal halide complexes, it is assumed that MAO attacks one of the CO ligands forming a carbene type complex [62,63]. A proof for this intermediate carbene complex would be the formation of polyacetylenes after adding acetylene. However, an oxidation step is required, since a carbocationic nickel center is usually proposed as the active species. Another possible pathway may be the release of both CO ligands followed

Table 4
Ethylene oligomerization results for the dinuclear and trinuclear complexes **3**, **4**, **6a**, and **7** (solvent: 250 mL *n*-pentane, activator: MAO, 10 bar ethylene, 60 °C, 1 h; for heterogeneous reactions, 2.0 g of silica was applied as support material). The contents of butenes (C4), hexenes (C6) and higher hydrocarbons were calculated from the GC integrals.

Entry	Complex	Al:Ni	Reaction Type	Activity (kg prod/mol Ni h)	∑C4 (%)	∑C6 (%)	∑ ⩾ C8 (%)
1	**3**	–	blank test	–	–	–	–
2	**4**	–	blank test	–	–	–	–
3	**6a**	–	blank test	–	–	–	–
4	**7**	–	blank test	–	–	–	–
5	**3**	2500	homogeneous	–	–	–	–
6	**4**	2500	homogeneous	290	28	68	4
7	**4**	250	homogeneous	81	31	63	6
8	**4**	250[a]	homogeneous	52	45	48	7
9	**6a**	2500	homogeneous	–	–	–	–
10	**7**	2500	homogeneous	–	–	–	–
11	**3**	250	heterogeneous	131	67	25	8
12	**4**	400	heterogeneous	206	47	40	13
13	**4**	250	heterogeneous	355	89	10	traces
14	**4**	230	heterogeneous	225	69	22	9
15	**4**	50	heterogeneous	129	59	27	14
16	**6a**	250	heterogeneous	181	62	24	14
17	**7**	250	heterogeneous	660	54	33	12

[a] Reaction conducted at 20 °C.

Table 5
Crystal and structure refinement data for complexes **3**, **4**, **6a**, and **7**.

	3	**4**	**6b**	**7** · CH_2Cl_2
Formula weight	512.93	855.11	895.94	754.01
Chemical formula	$C_{25}H_{19}FeNiO_3P$	$C_{46}H_{38}Fe_2NiO_2P_2$	$C_{44}H_{36}FeNi_2O_6P_2$	$C_{37}H_{30}Cl_2FeNiO_2P_2$
Crystal system	triclinic	triclinic	triclinic	monoclinic
Space group	$P\bar{1}$	$P\bar{1}$	$P\bar{1}$	$P2_1/c$
a (Å)	9.8541(4)	10.4428(6)	13.1526(13)	9.1954(10)
b (Å)	13.6595(5)	12.2856(6)	13.5622(13)	18.495(3)
c (Å)	18.2094(7)	16.8503(9)	20.297(2)	19.327(3)
α (°)	95.8440(10)	70.2800(10)	80.153(2)	90
β (°)	96.7360(10)	73.3520(10)	85.661(2)	91.900(4)
γ (°)	110.4530(10)	73.4920(10)	81.632(2)	90
V (Å^3)	2253.64(15)	1907.15(18)	3524.5(6)	3285.0(7)
ρ_{calc} (g cm^{-3})	1.512	1.489	1.266	1.525
F(0 0 0)	1048	880	1380	1544
Crystal size dimensions (mm)	0.3 × 0.2 × 0.2	0.2 × 0.1 × 0.01	0.3 × 0.2 × 0.2	0.4 × 0.2 × 0.2
Z	4	2	3	4
Index ranges	$-13 \leqslant h \leqslant 12$, $-18 \leqslant k \leqslant 18$, $0 \leqslant l \leqslant 24$	$-12 \leqslant h \leqslant 13$, $-14 \leqslant k \leqslant 15$, $0 \leqslant l \leqslant 21$	$-16 \leqslant h \leqslant 16$, $-16 \leqslant k \leqslant 16$, $0 \leqslant l \leqslant 25$	$-11 \leqslant h \leqslant 11$, $0 \leqslant k \leqslant 23$, $0 \leqslant l \leqslant 24$
μ (mm^{-1})	1.574	1.362	1.206	1.308
T (K)	203	203	293	188
θ (°)	1.14–28.30	1.80–26.37	1.54–26.52	1.52–26.44
Total reflections	59483	24813	41145	11733
Unique reflections	11 138	7778	14 419	5951
R_{int} (%)	3.90	8.10	4.58	10.30
Data/restraints/parameters	11138/0/559	7778/0/478	14419/0/751	5951/0/406
R_1, wR_2 [$I \geqslant \sigma(I)$][a]	0.0363, 0.0785	0.0532, 0.1025	0.0567, 0.1627	0.0735, 0.1373
R_1, wR_2 (all data)[a]	0.0573, 0.0864	0.1038, 0.1181	0.0986, 0.1875	0.1561, 0.1647
Godness-of-fit on F^2[b]	1.018	1.005	1.019	1.016
$\Delta\rho$(e Å^{-3})	0.428, −0.269	0.388, −0.374	1.158, −0.371	0.893, −0.651

[a] $R_1 = \frac{\sum_{hkl}||F_o|-|F_c||}{\sum_{hkl}|F_o|}$, $wR_2 = \sqrt{\frac{\sum_{hkl}w(F_o^2-F_c^2)^2}{\sum_{hkl}w(F_o^2)^2}}$, $w = \frac{1}{\sigma^2(F_o^2)+(a\cdot P)^2+b\cdot P}$, $P = \frac{\max(0,F_o^2)+2\cdot F_c^2}{3}$.

[b] GOF $= \sqrt{\frac{\sum_{hkl}w(F_o^2-F_c^2)^2}{m-n}}$, m = number of reflections, n = parameters used.

by an oxidative addition as described for a series of α-nitroketone [64] or salicylaldimine nickel catalysts [65] which is formulated to be the initial reaction sequence in nickel mediated polymerization of acetylenes [66].

Yellow solutions of **3**, **4**, **6a**, and **7** turn dark red after addition of MAO (Fig. 6a and b). Homogeneous ethylene oligomerization runs were performed for one hour under an ethylene pressure of 10 bar at 60 °C unless otherwise indicated (Table 4).

Complex **4** was the only candidate that showed oligomerization activity under homogeneous reaction conditions. Its activity was calculated to 290 kg prod/mol Ni h. The product mixture mainly consists of C6 isomers and lower amounts of C4 isomers. Higher olefins were only detected in traces. According to the theoretical discussion above, the Tolman cone angle seems to be a more reliable parameter to predict oligomerization activities than the P–Ni–P bite angle, as **7** is totally inactive (vide supra).

Previously Kamer and coworkers showed a clear relationship between the steric bulk of substituted pyridine–phosphane ligands and their performance in nickel mediated ethylene oligomerization—the turnover frequency increases with increasing steric bulk, as long as the nickel complexes are not overcrowded. Furthermore, the selectivity to 1-butene dropped significantly [67,68].

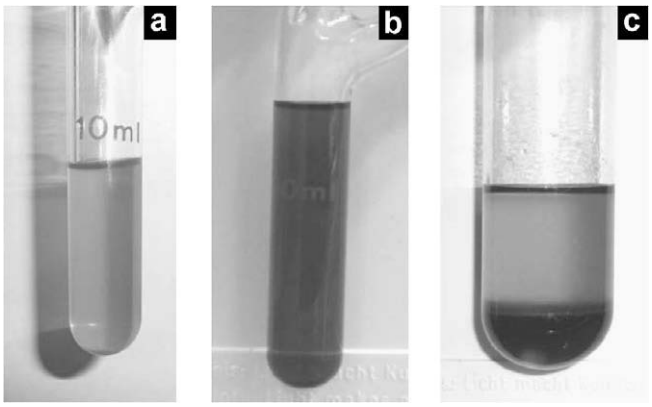

Fig. 6. (a) Catalyst solution in toluene. (b) Catalyst activated with MAO for homogeneous oligomerizations. (c) Heterogenized catalyst on silica (the color of the solution faded indicating the successful heterogenization). For a colored version of Fig. 6 see Supplementary material.

Most likely nickel complexes bearing sterically demanding phosphane ligands may react *via* tricoordinated species. This hypothesis would either explain the higher catalytic activity—just for steric reasons monophosphane nickel complexes favor the coordination of monomer molecules, the activation barrier for the insertion of ethylene monomers into the nickel–alkyl bond should be lower—or the decreasing selectivity towards 1-butene—a decrease in steric bulk by dissociation of one phosphane would allow further isomerization steps. Such monophosphane pathways are well established in homogeneous catalysis, e.g. the Suzuki coupling [69–75].

At a lower Al:Ni ratio, the activity dropped, while the selectivity to C4 hydrocarbons remained nearly constant (entries 6–8, Table 4) and mainly (>60%) hexenes were formed. When the experiment was performed at room temperature with a low aluminum:nickel ratio an increase in the formation of butenes was observed.

The inactivity of **3** and **6a** is in accordance with the observation that $[Ni(PBu_3)(CO)_3]$ does not catalyze either the isomerization nor the oligomerization of ethylenes in presence of alkylaluminum reagents [76].

For heterogeneous ethylene oligomerization reactions, MAO was added separately to a suspension of silica (GRACE, Davicat SI 1102, dried at 350 °C) and to a solution of the corresponding nickel complex. After methane evolution ceased—which was observed, when MAO was added to the silica suspension—the activated catalyst solution was combined with the silica/MAO mixture. The resulting heterogenous catalysts were washed and dried in vacuo to free flowing brownish or reddish powders (Fig. 6c).

Surprisingly, all complexes are potentially suitable as heterogeneous ethylene oligomerization catalysts. The highest activity of 660 kg prod /mol Ni h was achieved with **7** (entry 17, Table 4), while the residual complexes exhibited distinctively lower activities between 130 and 350 kg prod/mol Ni h, respectively. Interestingly, the selectivities toward C4 or C6 hydrocarbons have changed dramatically as determined by GC and GC/MS analyses. In all experiments, the C4 fraction was dominant in the product mixtures, and less amounts of hexenes were obtained. The contents of olefins ⩾C8 in the product mixtures slightly increased in the heterogeneous oligomerization reactions. At an aluminum:nickel ratio of 250:1, the best selectivity (89%) toward butenes was realized with complex **4** (entry 13, Table 4). At higher (400:1, entry 12) or lower (50:1, entry 15, Table 4) Al:Ni ratios, both the activities

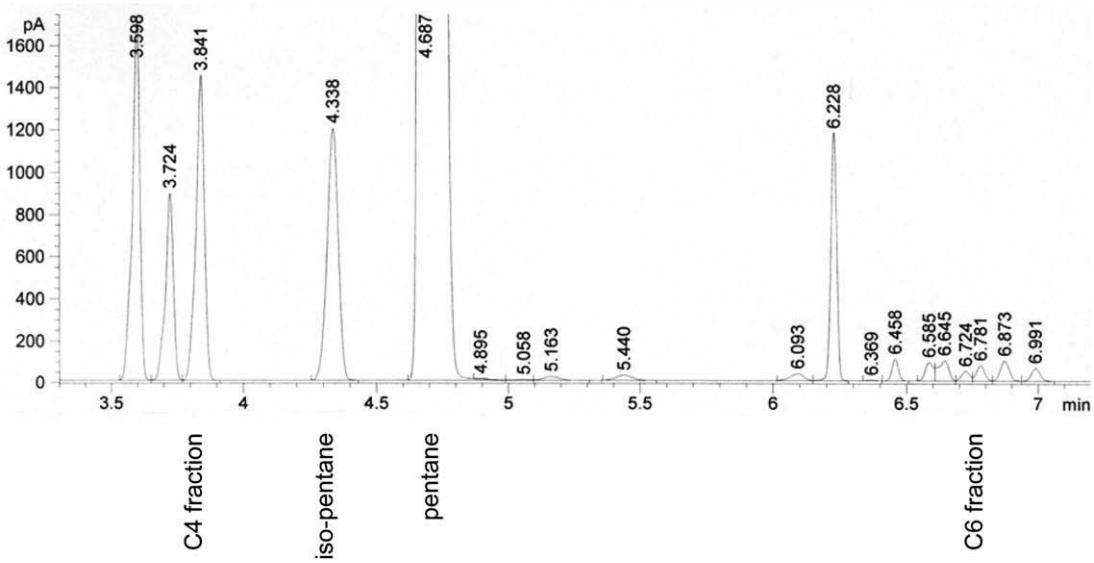

Fig. 7. GC spectrum of the C4–C6 region from a product mixture obtained with catalyst **6a**.

and selectivities of complex **4** decreased. The most active catalyst **7** showed only moderate selectivity to butenes.

According to the "core-shell" model, aluminoxane cages can be grown on the surfaces of appropriate support materials like silica. The support acts as a template [77–79] and favors the formation of MAO cages [80] leading to a distinctively higher number of cages compared with homogeneous solutions. As result thereof, the required amount of trimethylaluminum or MAO can be reduced dramatically. This effect was also observed for heterogenized complexes **3**, **4**, **6a**, and **7**. Coordination to the support surface seems to be responsible for the catalytic activity of all nickel carbonyls, therefore it is obvious that the Tolman cone angle is not suitable to predict activities of immobilized catalysts. It has been found previously that the catalytic productivity can be expressed by a complex function of e.g. the ligand structure, however those relationships can be quite different for analogous supported and unsupported species [81].

Fig. 7 shows a GC spectrum (C4/C6 region) obtained from the product mixture produced with complex **6a** (entry 16, Table 4) in which the peaks for the three butene isomers (1-butene, (*Z*)-2-butene, (*E*)-2-butene) are clearly separated. The "chain-running" mechanism can be postulated for these catalysts, since all possible isomers could be detected by GC or GC/MS (see especially the C6 fraction).

3. Conclusions

A series of bi- and trimetallic nickel(0) carbonyl complexes of type $[(FcPPh_2)_xNi(CO)_{4-x}]$ ($x = 1$, 2), $[(fc(PPh_2)_2)Ni(CO)_2]$, and $[fc(PR_2Ni(CO)_3)_2]$ (R = Ph, *p*-tolyl; Fc = $(\eta^5\text{-}C_5H_5)(\eta^5\text{-}C_5H_4)Fe$; fc = $(\eta^5\text{-}C_5H_4)_2Fe$) have been obtained by the reaction of $FcPPh_2$ or $fc(PR_2)_2$ (R = Ph, *p*-tolyl) with $Ni(CO)_4$. All compounds have been structurally characterized. Significant differences in the structural parameters of these compounds (e.g. the Tolman cone angles) have been outlined and discussed with respect to each other. In homogeneous ethylene oligomerization reactions it was found that only $[(FcPPh_2)_2Ni(CO)_2]$ (**4**) forms an active catalyst. Our investigations show that the influence of steric characteristics on the activity in ethylene oligo-/polymerization experiments can more seriously be predicted by the Tolman model rather than the bite angle concept. In heterogeneous experiments, chelate complex $[(fc(PPh_2)_2)Ni(CO)_2]$ (**7**) revealed the highest oligomerization activity but its selectivity toward C4 or C6 is only moderate. The selectivities to C4 and C6 were found to be completely different in heterogeneous reactions compared with the results of the homogeneous runs.

4. Experimental

4.1. General remarks

All reactions were carried out under an atmosphere of purified nitrogen (4.6) using standard Schlenk technique. Toluene, *n*-pentane and petroleum ether were purified by distillation from sodium; dichloromethane was purified by distillation from calcium hydride. Celite (purified and annealed, Erg. B.6, Riedel de Haen) was used for filtrations. $Ni(CO)_4$ was purchased from Aldrich and used as received. $FcPPh_2$, [82] $fc(PPh_2)_2$, [83] and $fc(P(p\text{-tolyl})_2)_2$ [83] were prepared according to published procedures. Infrared spectra were recorded with a Perkin Elmer FT-IR spectrometer Spectrum 1000. ^1H NMR spectra were recorded with a Bruker Avance 250 spectrometer operating at 250.130 MHz in the Fourier transform mode at 298 K. Chemical shifts are reported in δ units (*p*arts *p*er *m*illion) down-field from tetramethylsilane with the solvent as reference signal ($CDCl_3$: ^1H NMR $\delta = 7.26$). $^{31}P\{^1H\}$ NMR spectra were recorded at 101.249 MHz in $CDCl_3$ with $P(OMe)_3$ as external standard ($\delta = 139.0$) rel. to 85% H_3PO_4 ($\delta = 0.00$). Melting points of analytical pure samples (sealed off in nitrogen purged capillaries) were determined using a Gallenkamp MFB 595 010 M melting point apparatus. Microanalyses were performed using a Thermo FLASHEA 1112 Series instrument.

4.2. Synthesis of $[(FcPPh_2)Ni(CO)_3]$ (**3**)

$FcPPh_2$ (**1**) (200 mg, 0.540 mmol) was added in a single portion to a petroleum ether solution (20 mL) containing $Ni(CO)_4$ (**2**) (111 mg, 0.650 mmol) at 25 °C. The resulting reaction solution was stirred for 2.5 h at this temperature and was then filtered through a pad of celite. Afterward, all volatiles were removed in oil pump vacuum. Orange single crystals of **3** could be obtained by cooling a petroleum ether–toluene mixture (ratio 20:1, v/v, 10 mL) containing **3** to −30 °C. Yield: 221 mg (0.431 mmol, 80% based on **1**).

Mp. 103 °C. *Anal.* Calc. for $C_{25}H_{19}FeNiO_3P$ (512.93): C, 58.54; H, 3.73. Found: C, 58.54; H, 4.02%. IR (KBr): 2066 (s, ν_{CO}), 1984 (vs, ν_{CO}) cm^{-1}. ^1H NMR (250 MHz; $CDCl_3$; Me_4Si): δ_H 3.98 (bs, 5H, C_5H_5), 4.31 (bs, 2H, C_5H_4), 4.49 (bs, 2H, C_5H_4), 7.00–7.70 (m, 10H, C_6H_5) ppm. $^{31}P\{^1H\}$ NMR (101 MHz; $CDCl_3$; $P(OMe)_3$): δ_P 23.0 ppm.

4.3. Synthesis of $[(FcPPh_2)_2Ni(CO)_2]$ (**4**)

$[(FcPPh_2)Ni(CO)_3]$ (**3**) (50 mg, 0.097 mmol) and $FcPPh_2$ (**1**) (36 mg, 0.097 mmol) were dissolved in 10 mL of petroleum ether and stirred for 2 h at 25 °C. During this time a yellow solid precipitated. Decanting the solvent and washing the solid with petroleum ether (2 × 4 mL) gave the title complex. Single crystals of **4** could be obtained by cooling a dichloromethane–toluene mixture (ratio 20:1, v/v, 10 mL) containing **4** to −30 °C. Yield: 31 mg (0.036 mmol, 37% based on **3**).

Mp: 137 °C. IR (KBr): 1989(s, ν), 1927 (vs, ν_{CO}) cm^{-1}. ^1H NMR (250 MHz; $CDCl_3$; Me_4Si): δ_H 4.07–4.47 (m, 18H, C_5H_5 and C_5H_4), 7.00–7.77 (m, 20H, C_6H_5) ppm. $^{31}P\{^1H\}$ NMR (101 MHz; $CDCl_3$; $P(OMe)_3$): δ_P 28.7 ppm.

4.4. Synthesis of $[fc(PPh_2Ni(CO)_3)_2]$ (**6a**)

$fc(PPh_2)_2$ (**5a**) (100 mg, 0.180 mmol) was added in a single portion to a petroleum ether–toluene solution (ratio 2:1, v/v, 30 mL) containing **2** (74 mg, 0.433 mmol) at 25 °C. After 30 min of stirring at this temperature, 10 mL of toluene was added. Stirring was continued for 18 h. After filtration through a pad of celite, all volatiles were removed in oil pump vacuum. Orange single crystals of **6a** were obtained by cooling a petroleum ether–toluene mixture (ratio 20:1, v/v, 10 mL) containing **6a** to −30 °C. Yield: 95 mg (0.113 mmol, 63% based on **5a**).

Mp: 152 °C. *Anal.* Calc. for $C_{40}H_{28}FeNi_2O_6P_2$ (839.83): C, 57.21; H, 3.36. Found: C, 56.84; H, 3.71%. IR (KBr): 2067 (s, ν_{CO}), 1985 (vs, ν_{CO}) cm^{-1}. ^1H NMR (250 MHz; $CDCl_3$; Me_4Si): δ_H 3.98 (bs, 4H, C_5H_4), 4.27 (bs, 4H, C_5H_4), 7.00–7.70 (m, 20H, C_6H_5) ppm. $^{31}P\{^1H\}$ NMR (101 MHz; $CDCl_3$; $P(OMe)_3$): δ_P 22.6 ppm.

4.5. Synthesis of $[fc(P(p\text{-tolyl})_2Ni(CO)_3)_2]$ (**6b**)

$Fc(P(p\text{-tolyl})_2)_2$ (100 mg, 0.164 mmol) (**5b**) and **2** (67 mg, 0.394 mmol) were reacted under the same reaction conditions as described for the synthesis of **6a** (vide supra). After appropriate work-up, compound **6b** could be isolated as a yellow solid. Yield: 113 mg (0.126 mmol, 77% based on **5b**).

Mp: 161 °C. Anal. Calc. for $C_{44}H_{36}FeNi_2O_6P_2$ (895.93): C, 58.99; H, 4.05%. Found: C, 58.93; H, 3.91%. IR (KBr): 2066 (s, ν_{CO}), 1980 (vs, ν_{CO}) cm^{-1}. ^1H NMR (250 MHz; $CDCl_3$; Me_4Si): δ_H 2.28 (s, 6H,

CH_3), 3.91–4.50 (m, 8H, C_5H_4), 6.59–7.66 (m, 16H, C_6H_5) ppm. $^{31}P\{^1H\}$ NMR (101 MHz; $CDCl_3$; $P(OMe)_3$): δ_P 19.7 ppm.

4.6. Synthesis of [(fc(PPh$_2$)$_2$)Ni(CO)$_2$] (7)

A new method for the preparation of **7** was developed: complex [fc($PPh_2Ni(CO)_3$)$_2$] (30 mg, 0.036 mmol) (**6a**) was dissolved in 10 mL of toluene and heated for 6 h to 40 °C. Afterward, the reaction mixture was filtered through a pad of celite and all volatiles were removed in oil pump vacuum. Molecule **7** could be obtained as a yellow solid after crystallization from a dichloromethane toluene mixture (ratio 20:1, v/v, 4 mL) at −30 °C. Yield: 10 mg (0.015 mmol, 42% based on **6a**).

IR (KBr): 2000 (s, ν_{CO}), 1943 (vs, ν_{CO}) cm^{-1}. ^1H NMR (250 MHz; $CDCl_3$; Me_4Si): δ_H 4.08 (bs, 4H, C_5H_4), 4.22 (bs, 4H, C_5H_4), 7.26–7.70 (m, 20H, C_6H_5) ppm. $^{31}P\{^1H\}$ NMR (101 MHz; $CDCl_3$; $P(OMe)_3$): δ_P 25.1 ppm.

4.7. Single crystal X-ray diffraction analysis

Crystal data for **3**, **4**, **6a**, and **7** are summarized in Table 5. All data were collected on a Bruker Smart CCD diffractometer at 203 (**3**, **4**), 293 (**6b**) or 188 K (**7**) using Mo Kα radiation (λ = 0.71073 Å). The structures were solved by direct methods using SHEXLS-97 [84] and refined by full-matrix least-square procedures on F^2 using SHELXL-97 [85]. All non-hydrogen atoms were refined anisotropically and a riding model was employed in the refinement of the hydrogen atom positions.

4.8. Homogeneous polymerization of ethylene in a 1 L Büchi autoclave

An amount of 5–25 mg of the respective complex was dissolved in 5 mL of toluene. Methylalumoxane (MAO) (10% in toluene) was added according to the desired Ni:Al ratio resulting in an immediate color change. The mixture was added to a 1 L Schlenk flask filled with 250 mL of *n*-pentane. This mixture was transferred to a 1 L Büchi laboratory autoclave under inert atmosphere and thermostated at 60 °C. An ethylene pressure of 10 bar was applied for 1 h. The reactor was cooled to ambient temperature and the pressure was released. To the oligomer solutions, diluted hydrochloric acid was added. The organic phase was separated and dried over sodium sulfate. *n*-Pentane was distilled off using a Vigreux column. The resulting oligomer mixtures were characterized using gas chromatography and GC/MS analyses.

Please, notice that for blank tests, the toluene solutions of the corresponding complexes were applied without addition of MAO.

4.9. Heterogeneous polymerization of ethylene in a 1 L Büchi autoclave

Silica (2.0 g, Davison, GRACE, SI 1102, dried at 350 °C) was suspended in 30 mL toluene. Half of the calculated amount of MAO was added to the silica suspension resulting in an immediate evolution of methane. An amount of 5–25 mg of the desired complex was dissolved in 5 mL of toluene and the residual amount of MAO was added by syringe resulting in a color change from yellow to dark red. The catalyst solution was combined with the silica/MAO suspension after methane evolution had ceased. After stirring for 2 h, the heterogeneous catalyst was filtered over a glass frit, washed twice with 10 mL portions of toluene and 10 mL of *n*-pentane and dried in vacuo to give a free flowing powder. Subsequently, the polymerization reactor was charged with 250 mL of *n*-pentane and the powdered catalyst under inert atmosphere and thermostated at 60 °C. An ethylene pressure of 10 bar was applied for 1 h. The reactor was cooled to room temperature and the pressure was released. To the oligomer solutions, diluted hydrochloric acid was added. The organic phase was separated and dried over sodium sulfate. *n*-Pentane was distilled off using a Vigreux column. The resulting oligomer mixtures were characterized using gas chromatography and GC/MS analyses.

4.10. Gas chromatography

GC/MS spectra were recorded with a Thermo Focus gaschromatograph in combination with a Thermo DSQ mass detector containing a TR-5MS column (5% phenyl(equiv)-polysilphenylenesiloxane; length: 30 m; film: 0.25 μm; flow: 200 mL/min, split: 200:1). Helium (4.6) was applied as carrier gas. The routinely used temperature program includes a starting phase (2 min at 50 °C), a heating phase (24 min; heating rate: 10 K/min; final temperature: 290 °C) and a plateau phase (15 min at 290 °C).

GC spectra were recorded on a gaschromatograph HP 6890N (Agilent) equipped with a HP-5 (5% phenyl–methyl–siloxane) column (length: 30 m; film: 1.5 μm; diameter: 0.53 mm). Using argon as the carrier gas, the flow was adjusted to 150 mL/min (split 50:1). The temperature program contains a starting phase (6 min at 35 °C), a heating phase (1 K/min for 10 min, then 20 K/min for 10 min) and the final plateau phase (20 min at 250 °C).

Acknowledgement

We are grateful to the Deutsche Forschungsgemeinschaft and the Fonds der Chemischen Industrie for generous financial support.

Appendix A. Supplementary material

CCDC 756889, 756890, 756891, and 756892 contain the supplementary crystallographic data for **3**, **4**, **6a**, and **7**. These data can be obtained free of charge from The Cambridge Crystallographic Data Centre via www.ccdc.cam.ac.uk/data_request/cif. Supplementary data associated with this article can be found, in the online version, at doi:10.1016/j.jorganchem.2010.03.012.

References

[1] W. Hodes, L. Meriwether, Patent US 3054775, 1962.
[2] J. Floss, N.v. Kutepow, Patent DE 1153904, 1963.
[3] C. Carlini, M. Marchionna, A. Galletti, G. Sbrana, J. Mol. Catal. A: Chem. 169 (2001) 19.
[4] F. Benvenuti, C. Carlini, M. Marchionna, R. Patrini, A. Galletti, G. Sbrana, Appl. Catal. A 199 (2000) 123.
[5] F. Benvenuti, C. Carlini, M. Marchionna, R. Patrini, A. Galletti, G. Sbrana, Appl. Catal. A 204 (2000) 7.
[6] S. Wu, S. Lu, Chin. Chem. Lett. 14 (2003) 958.
[7] S. Wu, S. Lu, Appl. Catal. A 246 (2003) 295.
[8] S. Wu, S. Lu, J. Mol. Catal. A: Chem. 198 (2003) 29.
[9] S. Wu, S. Lu, J. Mol. Catal. A: Chem. 197 (2003) 51.
[10] F. Benvenuti, C. Carlini, M. Marchionna, A. Galletti, G. Sbrana, J. Mol. Catal. A: Chem. 178 (2002) 9.
[11] M. Bluhm, C. Folli, D. Pufky, M. Kröger, O. Walter, M. Döring, Organometallics 24 (2005) 4139.
[12] P. Kuhn, D. Sémeril, D. Matt, M. Chetcuti, P. Lutz, Dalton Trans. 5 (2007) 515.
[13] J. Heinicke, M. Köhler, N. Peulecke, W. Keim, J. Catal. 225 (2004) 16.
[14] F. Speiser, P. Braunstein, L. Saussine, Organometallics 23 (2004) 2625.
[15] C. Carlini, M. Marchionna, R. Patrini, A. Galletti, G. Sbrana, Appl. Catal. A 216 (2001) 1.
[16] J. Pietsch, P. Braunstein, Y. Chauvin, New. J. Chem. 22 (1998) 467.
[17] F. Speiser, P. Braunstein, L. Saussine, Acc. Chem. Res. 38 (2005) 784.
[18] P. Wasserscheid, Synthetic Methods of Organometallic and Inorganic Chemistry, Thieme, Stuttgart, 2002.
[19] W. Keim, Angew. Chem., Int. Ed. Engl. 29 (1990) 235.
[20] M. Kranenburg, P. Kamer, P. van Leeuwen, D. Vogt, W. Keim, J. Chem. Soc., Chem. Commun. (1995) 2177.
[21] W. Goertz, W. Keim, D. Vogt, U. Englert, M. Boele, L. van der Veen, P. Kamer, P. van Leeuwen, J. Chem. Soc., Dalton Trans. (1998) 2981.
[22] B. Edelbach, D. Vicic, R. Lachicotte, W. Jones, Organometallics 17 (1998) 4784.
[23] C. Perthuisot, B. Edelbach, D. Zubris, N. Simhai, C. Iverson, C. Müller, T. Satoh, W. Jones, J. Mol. Catal. A: Chem. 189 (2002) 157.
[24] H. Yamanaka, K. Edo, F. Shoji, S. Konno, T. Sakamoto, M. Mizugaki, Chem. Pharm. Bull. 26 (1978) 2160.
[25] M. Elmoghayar, K. Undheim, Acta Chem. Scand. B37 (1983) 160.

[26] K. Tamao, J. Organomet. Chem. 653 (2002) 23.
[27] M. Uemura, H. Yorimitsu, K. Oshima, Chem. Commun. (2006) 4726.
[28] M. Fox, D. Chandler, Adv. Mater. 3 (1991) 381.
[29] R. Mercury, Patent WO 2007142662, 2007.
[30] L. Zhou, A. Rai, N. Piekiel, X. Ma, M. Zachariah, Chem. Phys. Process. Combust. (2007) C14.
[31] R. Mercury, Patent US 2007034050, 2007.
[32] E. Kauffeldt, T. Kauffeldt, J. Nanopart. Res. 8 (2006) 477.
[33] Y. He, X. Li, M. Swihart, Chem. Mater. 17 (2005) 1017.
[34] Z. Weng, S. Teo, L. Koh, T. Hor, Angew. Chem., Int. Ed. 44 (2005) 7560.
[35] K. Barnett, Patent US 4628139 A 19861209, 1986.
[36] Z. Weng, S. Teo, T. Hor, Organometallics 25 (2006) 4878.
[37] J. Yoo, Patent US 3992470 19761116, 1976.
[38] A.-H. Wu, Patent US 5237118 A 19930817, 1993.
[39] Z. Weng, S. Teo, Z.-P. Liu, T. Hor, Organometallics 26 (2007) 2950.
[40] S. Shimizu, A. Osuka, Chem. Commun. (2006) 1319.
[41] C. Tolman, J. Am. Chem. Soc. 92 (1970) 2956.
[42] G. Vasapollo, L. Toniolo, G. Cavinato, F. Bigoli, M. Lanfranchi, M. Pellinghelli, J. Organomet. Chem. 481 (1994) 173.
[43] B. Hamann, J. Hartwig, J. Am. Chem. Soc. 120 (1998) 3694.
[44] C. Elschenbroich, A. Salzer, Organometallchemie, Teubner, Studienbücher, Stuttgart, 1993.
[45] C. Tolman, J. Am. Chem. Soc. 92 (1970) 2953.
[46] H. Lang, B. Lühmann, R. Buschbeck, J. Organomet. Chem. 689 (2004) 3598.
[47] C. Tolman, Chem. Rev. 77 (1977) 313.
[48] H. Han, M. Elsmaili, S.A. Johnson, Inorg. Chem. 45 (2006) 7435.
[49] M.O. Sinnokrot, E.F. Valeev, C.D. Sherrill, J. Am. Chem. Soc. 124 (2002) 10887.
[50] C. Elschenbroich, M. Wünsch, A. Behrend, B. Metz, B. Neumüller, K. Harms, Organometallics 24 (2005) 5509.
[51] T. Baumgartner, P. Moors, M. Nieger, H. Hupfer, E. Niecke, Organometallics 21 (2002) 4919.
[52] A. Jakob, B. Milde, P. Ecorchard, C. Schreiner, H. Lang, J. Organomet. Chem. 693 (2008) 3821.
[53] R.B. DeVasher, J.M. Spruell, D.A. Dixon, G.A. Broker, S.T. Griffin, R.D. Rogers, K.H. Shaughnessy, Organometallics 24 (2005) 962.
[54] J.W. Gosselink, H. Bulthuis, G. van Koten, J. Chem. Soc., Dalton Trans. 6 (1981) 1342.
[55] B.C. Taverner, J. Comput. Chem. 17 (1996) 1612.
[56] B.C. Taverner, Steric, 1.11, 1995 <http://www.ccl.net/cca/software/SOURCES/C/steric/index.shtml>.
[57] G. Wilkinson, R.D. Gillard, J.A. McCleverty, Comprehensive Coordination Chemistry, second ed., Pergamon Press, Oxford, 1987.
[58] P.W.N.M. van Leeuwen, P.C.J. Kamer, J.N.H. Reek, P. Dierkes, Chem. Rev. 100 (2000) 2741.
[59] I. Albers, E. Álvarez, J. Cámpora, C.M. Maya, P. Palma, L.J. Sánchez, E. Passaglia, J. Organomet. Chem. 689 (2004) 833.
[60] I.R. Butler, W.R. Cullen, T.-J. Kim, S.J. Rettig, J. Trotter, Organometallics 4 (1985) 972.
[61] W.H. Watson, A. Nagl, M.-J. Don, M.G. Richmond, J. Chem. Cryst. 29 (1999) 871.
[62] P.C. Casey, C.R. Cyr, R.A. Boggs, Synth. Inorg. Metal–Org. Chem. 3 (1973) 249.
[63] C.T. Lam, C.D. Malkiewich, C.V. Senoff, Inorg. Synth. (1977) 95.
[64] C. Carlini, M. Marchionna, A.M.R. Galletti, G. Sbrana, Appl. Catal. A 210 (2001) 173.
[65] C. Carlini, A.M.R. Galletti, G. Sbrana, Polymer 44 (2003) 1995.
[66] L.S. Meriwether, M.F. Leto, E.C. Colthup, G.W. Kennerly, J. Org. Chem. 27 (1962) 3930.
[67] J. Flapper, P.W.N.M. van Leeuwen, C.J. Elsevier, P.C.J. Kamer, Organometallics 28 (2009) 3264.
[68] J. Flapper, H. Kooijman, M. Lutz, A.L. Spek, P.W.N.M. van Leeuwen, C.J. Elsevier, P.C.J. Kamer, Organometallics 28 (2009) 3272.
[69] Z. Li, Y. Fu, Q.-X. Guo, L. Liu, Organometallics 27 (2008) 4043.
[70] E. Galardon, S. Ramdeehul, J.M. Brown, A. Cowley, K.K.M. Hii, A. Jutand, Angew. Chem., Int. Ed. 41 (2002) 1760.
[71] F. Barrios-Landeros, J.F. Hartwig, J. Am. Chem. Soc. 127 (2005) 6944.
[72] J.P. Stambuli, M. Bühl, J.F. Hartwig, J. Am. Chem. Soc. 124 (2002) 9346.
[73] J.P. Stambuli, C.D. Incarvito, M. Bühl, J.F. Hartwig, J. Am. Chem. Soc. 126 (2004) 1184.
[74] T.E. Barder, S.D. Walker, J.R. Martinelli, S.L. Buchwald, J. Am. Chem. Soc. 127 (2005) 4685.
[75] T.E. Barder, M.R. Biscoe, S.L. Buchwald, Organometallics 26 (2007) 2183.
[76] L.M. Clutterbuck, L.D. Field, G.B. Humphries, A.F. Masters, M.A. Williams, Appl. Organomet. Chem. 4 (1990) 507.
[77] M. Helldörfer, H.G. Alt, J. Ebenhoch, J. Appl. Polym. Sci. 86 (2002) 3021.
[78] W.-R. Schmeal, J.-R. Street, AlChE J. 17 (1971) 1188.
[79] E.J. Nagel, V.A. Kirillov, W.H. Ray, Ind. Eng. Chem. Prod. Res. Dev. 19 (1980) 372.
[80] E. Zurek, T.K. Woo, T.K. Firman, T. Ziegler, Inorg. Chem. 40 (2001) 3619.
[81] S.D. Ittel, L.K. Johnson, Chem. Rev. 100 (2000) 1169.
[82] G.P. Sollott, H.E. Mertwoy, S. Portnoy, J.L. Snead, J. Org. Chem. 28 (1963) 1090.
[83] J.J. Bishop, A. Davidson, M.L. Katcher, D.W. Lichtenberg, R.E. Merrill, J.C. Smart, J. Organomet. Chem. 27 (1971) 241.
[84] G.M. Sheldrick, Acta Crystallogr., Sect. A 46 (1990) 467.
[85] G.M. Sheldrick, SHELXL-97 Program for Crystal Structure Refinement, Universität Göttingen, 1997.